Appendix 1
Assessing the impact of non-pharmaceutical interventions on SARS-CoV-2 transmission in Switzerland

Joseph. C. Lemaitre[1,*], Javier Perez-Saez[2,*], Andrew S. Azman[2], Andrea Rinaldo[1,3], and Jacques Fellay[4,5]

[1] *Laboratory of Ecohydrology, School of Architecture, Civil and Environmental Engineering, École Polytechnique Fédérale de Lausanne, CH-1015 Lausanne*
[2] *Department of Epidemiology, Johns Hopkins Bloomberg School of Public Health, Baltimore, Maryland, USA*
[3] *Dipartimento di Ingegneria Civile Edile ed Ambientale, Università di Padova, I-35131 Padua, Italy*
[4] *School of Life Sciences, École Polytechnique Fédérale de Lausanne, CH-1015 Lausanne*
[5] *Precision Medicine Unit, Lausanne University Hospital and University of Lausanne, CH-1011 Lausanne*
[*] *Share first authorship*

1 Canton of Vaud hospitalization data

We had access to individual-level data from 1093 patients hospitalized in the canton of Vaud up to April 14th. Of all patient 41% (448/1093) where female and 59% were male (645/1093). The median age was 70 years old (Supplementary Material, SM, Figure 1). The proportion of patients requiring Intensive Care Units (ICUs) was of 20% (214/1093).

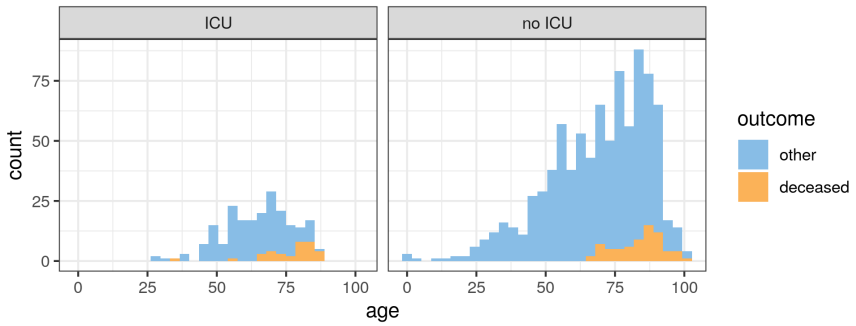

SM Figure 1: Age distribution of patients hospitalized for COVID-19 in the canton of Vaud up to April 14.

Of 777 patients with known outcome on April 14, 104 had deceased (13%). We estimate the hospitalization Case Fatality Ratio (hCFR) by adjusting for the distribution of time hospitalization to death following Nishiura et al. 2009:

$$hCFR(t) = \frac{D(t)}{\int_0^t C(\tau) f(t-\tau) d\tau}$$

where $D(t)$ and $C(t)$ are the cumulative number of deaths at time t, and $f(u)$ is the PDF of the time from hospitalization to death. We estimate $f(t)$ from the data assuming a log-normal distribution. The estimated hCFR was of 11% (95% CI: 10%-14%) in the four days up to the last observation on April 14 (SM Figure 2).
The distribution of times of hospitalization processes are shown in SM Figure 3, and fitted distribution parameters given in 1.

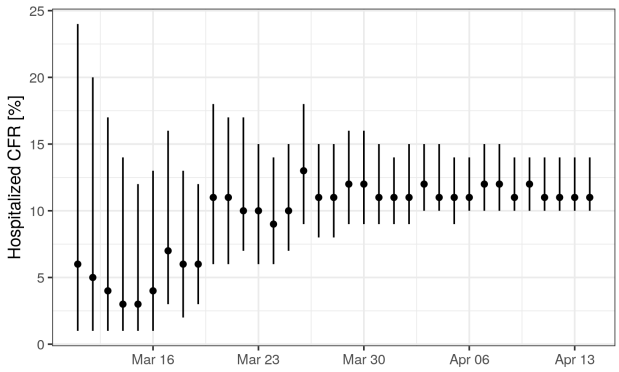

SM Figure 2: Estimated hospitalized Case Fatality Ratio using method from Nishiura et al. 2009,

SM Table 1: Estimated parameters of hospitalization time distributions. All times are in days and taken from the date of hospitalization if not specified otherwise.

	mean	sd	mean (logscale)	sd (logscale)
Time hospitalized	8.49	6.58	1.81	0.87
Time to death	8.23	6.09	1.80	0.87
Time to discharge without ICU	6.29	4.66	1.56	0.80
Time hospitalized without ICU	7.35	5.79	1.68	0.85
Time to death without ICU	7.84	6.27	1.73	0.88
Time to ICU	2.35	3.79	0.18	1.05
Time hospitalized with ICU	13.14	7.50	2.37	0.72
Time in ICU	8.36	6.76	1.69	1.04
Time from ICU to discharge	8.68	6.99	1.71	1.07
Time from ICU to death	6.97	4.98	1.68	0.77

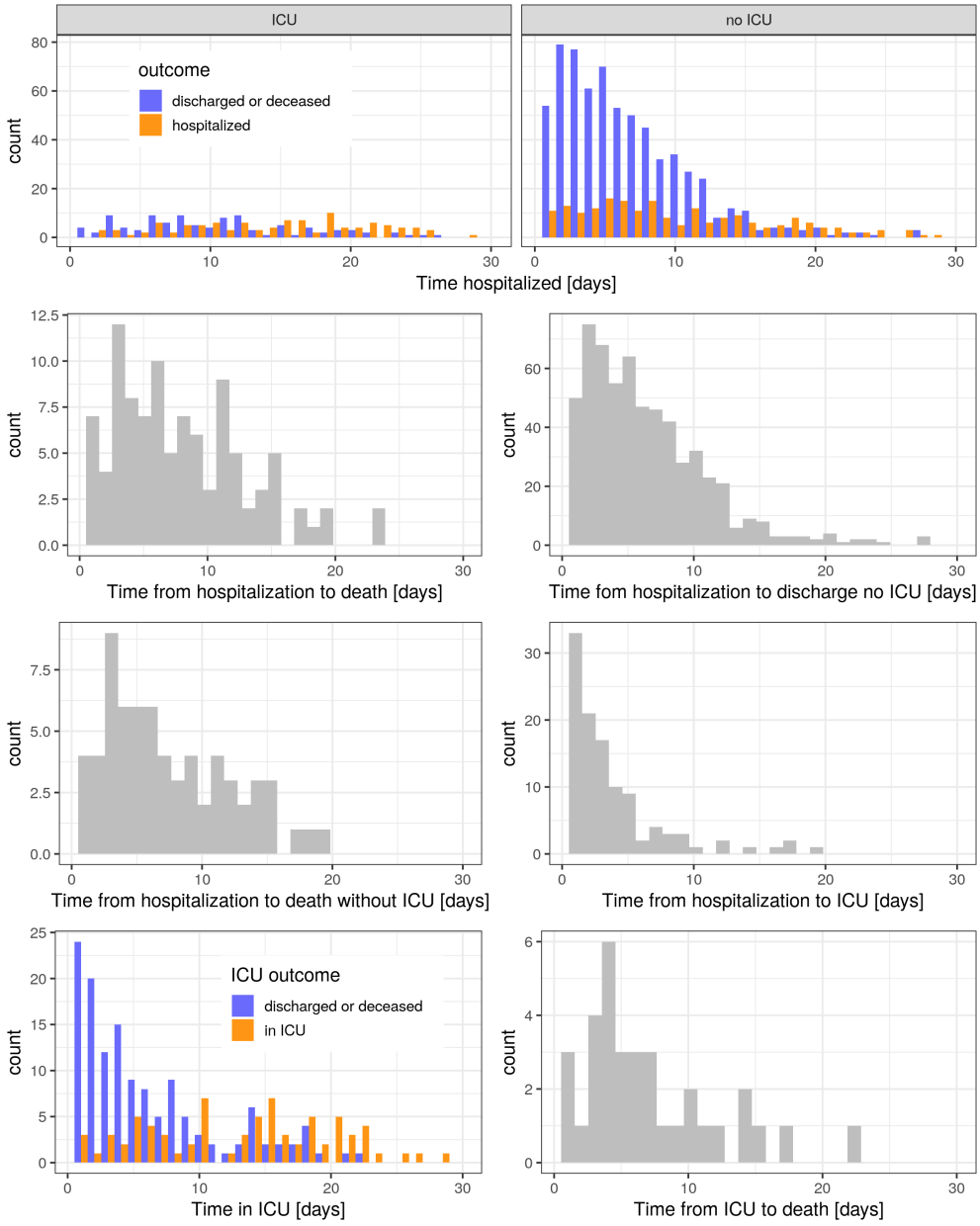

SM Figure 3: Histograms of times to key hospitalization events. Data from canton of Vaud.

2 Model Description

We build a COVID-19 compartmental transmission model based on the Susceptible Exposed Infected Recovered (SEIR) template with three I compartments. The schematic with the different transitions and compartments is shown in SM Figure 4. Infected individuals have some probability of developing severe symptoms which require hospitalization after a delay from symptom onset (I_h). Hospitalization can lead to recovery or death, either through normal hospitalization ($H_{a,b}$ and H_d respectively) or passing through Intensive Care Units (ICUs) ($U_{a,b}$ and U_d respectively). We divide some compartments in two sub-compartments, denoted by subscripts a, b, to capture the bimodal time distributions. Data from the canton of Vaud show a high proportion of deaths outside of hospitals ($\approx 50\%$), we therefore also include a pathway from infection to death without passing through hospitalization (I_d).

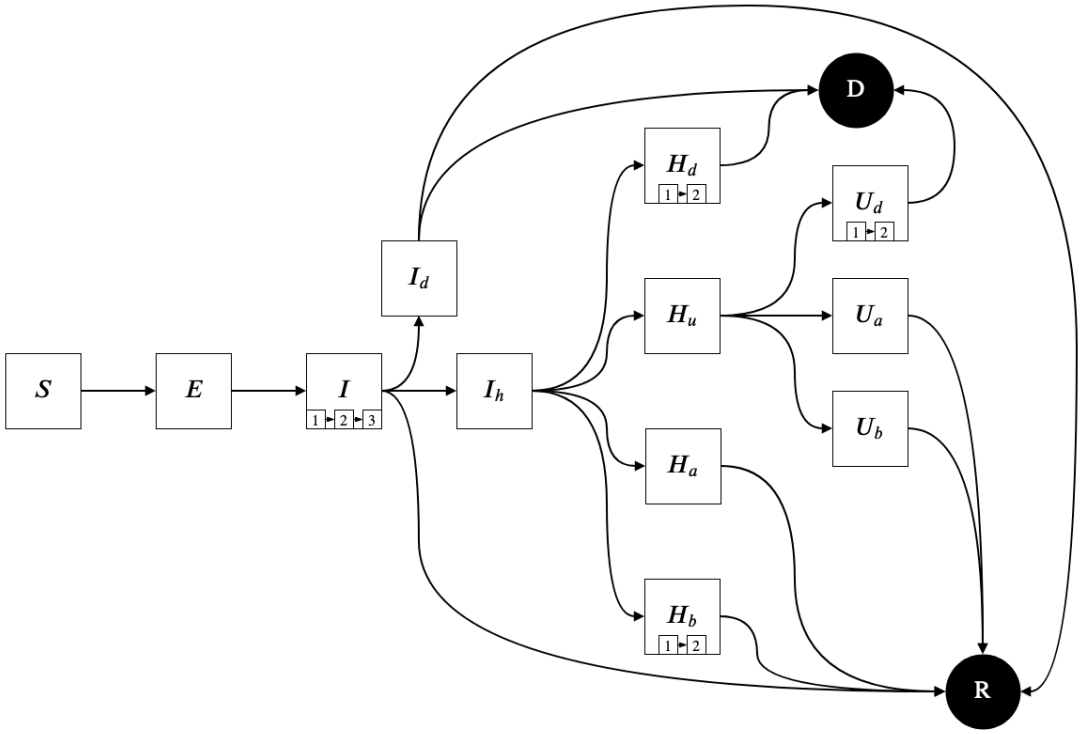

SM Figure 4: Schematic diagram of COVID-19 transmission and hospitalization processes. There is two sinks: Death D and recovered R. Each stage with regard to the disease may be implemented with several compartments (little numbered boxes) to better represent the time distribution spent in that stage. Branching between stages denoted by a, b are used to characterized bi-modal distributions of ICU and hospital stays.

The time spent in the observable hospitalization states were used to define the number of stages in each compartment by fitting Erlang distributions to the data of canton de Vaud. During this process we found that for the time to recovery for hospitalizations, t_h, and ICUs, t_u mixture models with two groups of patients had stronger support than a single distribution for all patients. We therefore fit for both of these groups Erlang mixture models formulated as:

$$t_h \sim \theta_h \text{Erlang}(k_{h,a}, \lambda_{h,a}) + (1 - \theta_h)\text{Erlang}(k_{h,b}, \lambda_{h,b})$$
$$t_u \sim \theta_u \text{Erlang}(k_{u,a}, \lambda_{u,a}) + (1 - \theta_u)\text{Erlang}(k_{u,b}, \lambda_{u,b}),$$

where $\theta_{h,u}$ are the probabilities of patients being in their respective group a, and k and λ are respectively the shape and rate parameters of the Erlang distribution. We fit the Erlang mixture models in a Bayesian framework using Stan Carpenter et al. 2017. For inference we parameterize the model in terms of the mean stay in each compartment $\mu = k/\lambda$. Results are shown in Table 2.

SM Table 2: Posterior parameters of Erlang mixture distributions for times from hospitalization and ICU to recovery. We report the mean and 95% credible intervals (in parenthesis) of the posterior distributions of the probability of patients being of group a, θ, the shape parameter (equal to the number of stages per compartment), k, and the mean time spent in each state, μ.

		Group a		Group b	
Compartment	θ	k	μ	k	μ
Hospitalized to recovery $H_{a,b}$	0.34 (0.26-0.43)	1	3.0 (2.5-3.6)	2	9.4 (8.7-10.2)
ICU to recovery $U_{a,b}$	0.33 (0.21-0.44)	1	2.9 (2.1-3.8)	1	13.7 (12.1-15.4)

We therefore use either one (stage H_a, U_a, U_b) or two (stages H_d, H_b, U_d) compartments for each stage based on estimated shape parameters of the Erlang distributions. With just one compartment, we obtain an exponentially distributed transmission time. Rates of transitions are shown Table 3 and branching probabilities in Table 4.

2.1 Model equations

The model has been implemented as a discrete-state model based on a Partially-Observed Markov Process (POMP), simulating the transitions between compartments as discrete events using stochastic count processes King et al. 2008; Bretó et al. 2009. Let $N_{AB}(t)$ be the number of individuals transiting between compartments $A, B \in \mathcal{X}$ in the time interval $[0, t)$ where $\mathcal{X}$ is the state vector,

$$\mathcal{X} = \{S, E, I^{1,2,3}, I_d, I_h, H_a, H_b^{1,2}, H, U_a, U_b, H_d^{1,2}, U_d^{1,2}, R, D\}$$

The number of transitions during a time-step Δt is $\Delta N_{AB}(t) = N_{AB}(t + \Delta t) - N_{AB}(t)$. We model time-varying $R_0(t) = \beta(t)/(3r_I)$ as a geometric random walk defined by its calibrated variance, where β is the transmission parameter and $1/(3r_I)$ is the mean duration spent in the infectious compartments $I^1 to I^3$. The force of infection is expressed in terms of $\beta(t)$ in the model. Given the state of the system at time t, $\mathcal{X}_t$, the model reads:

$$
\begin{aligned}
\mathbb{P}\left[\Delta N_{SE}(t)=1\middle|\,\mathcal{X}_t\right] &= \beta(t)\frac{I^1(t)+I^2(t)+I^3(t)}{P}S(t)\Delta t+o(\Delta t)\\
\mathbb{P}\left[\Delta N_{EI^1}(t)=1\middle|\,\mathcal{X}_t\right] &= r_E E(t)\Delta t+o(\Delta t)\\
\mathbb{P}\left[\Delta N_{I^1I^2}(t)=1\middle|\,\mathcal{X}_t\right] &= 3r_I I^1(t)\Delta t+o(\Delta t)\\
\mathbb{P}\left[\Delta N_{I^2I^3}(t)=1\middle|\,\mathcal{X}_t\right] &= 3r_I I^2(t)\Delta t+o(\Delta t)\\
\mathbb{P}\left[\Delta N_{I^3I_d}(t)=1\middle|\,\mathcal{X}_t\right] &= p_{I_d|I^3}\cdot 3r_I I^3(t)\Delta t+o(\Delta t)\\
\mathbb{P}\left[\Delta N_{I^3I_h}(t)=1\middle|\,\mathcal{X}_t\right] &= p_{I_h|I^3}\cdot 3r_I I^3(t)\Delta t+o(\Delta t)\\
\mathbb{P}\left[\Delta N_{I^3R}(t)=1\middle|\,\mathcal{X}_t\right] &= p_{R|I^3}\cdot 3r_I I^3(t)\Delta t+o(\Delta t)\\
\mathbb{P}\left[\Delta N_{I_dR}(t)=1\middle|\,\mathcal{X}_t\right] &= p_{R|I_d}\cdot r_I I_d(t)\Delta t+o(\Delta t)\\
\mathbb{P}\left[\Delta N_{I_dD}(t)=1\middle|\,\mathcal{X}_t\right] &= p_{D|I_d}\cdot r_I I_d(t)\Delta t+o(\Delta t)\\
\mathbb{P}\left[\Delta N_{I_hH_d^1}(t)=1\middle|\,\mathcal{X}_t\right] &= p_{H_d|I_h}\cdot r_{I_h} I_h(t)\Delta t+o(\Delta t)\\
\mathbb{P}\left[\Delta N_{I_hH_u}(t)=1\middle|\,\mathcal{X}_t\right] &= p_{H_u|I_h}\cdot r_{I_h} I_h(t)\Delta t+o(\Delta t)\\
\mathbb{P}\left[\Delta N_{I_hH_a}(t)=1\middle|\,\mathcal{X}_t\right] &= p_{H_a|I_h}\cdot r_{I_h} I_h(t)\Delta t+o(\Delta t)\\
\mathbb{P}\left[\Delta N_{I_hH_b^1}(t)=1\middle|\,\mathcal{X}_t\right] &= p_{H_b|I_h}\cdot r_{I_h} I_h(t)\Delta t+o(\Delta t)\\
\mathbb{P}\left[\Delta N_{H_aR}(t)=1\middle|\,\mathcal{X}_t\right] &= r_{H_a} H_a(t)\Delta t+o(\Delta t)\\
\mathbb{P}\left[\Delta N_{H_b^1H_b^2}(t)=1\middle|\,\mathcal{X}_t\right] &= 2r_{H_b} H_b^1(t)\Delta t+o(\Delta t)\\
\mathbb{P}\left[\Delta N_{H_b^2R}(t)=1\middle|\,\mathcal{X}_t\right] &= 2r_{H_b} H_b^2(t)\Delta t+o(\Delta t)\\
\mathbb{P}\left[\Delta N_{H_uU_d^1}(t)=1\middle|\,\mathcal{X}_t\right] &= p_{U_d|H_u}\cdot r_{H_u} H_u(t)\Delta t+o(\Delta t)\\
\mathbb{P}\left[\Delta N_{H_uU_a}(t)=1\middle|\,\mathcal{X}_t\right] &= p_{U_a|H_u}\cdot r_{H_u} H_u(t)\Delta t+o(\Delta t)\\
\mathbb{P}\left[\Delta N_{H_uU_b}(t)=1\middle|\,\mathcal{X}_t\right] &= p_{U_b|H_u}\cdot r_{H_u} H_u(t)\Delta t+o(\Delta t)\\
\mathbb{P}\left[\Delta N_{H_d^1U_d^2}(t)=1\middle|\,\mathcal{X}_t\right] &= 2r_{H_d} H_d^1(t)\Delta t+o(\Delta t)\\
\mathbb{P}\left[\Delta N_{H_d^2D}(t)=1\middle|\,\mathcal{X}_t\right] &= 2r_{H_d} H_d^2(t)\Delta t+o(\Delta t)\\
\mathbb{P}\left[\Delta N_{U_aR}(t)=1\middle|\,\mathcal{X}_t\right] &= r_{U_a} U_a(t)\Delta t+o(\Delta t)\\
\mathbb{P}\left[\Delta N_{U_bR}(t)=1\middle|\,\mathcal{X}_t\right] &= r_{U_b} U_b(t)\Delta t+o(\Delta t)\\
\mathbb{P}\left[\Delta N_{U_d^1U_d^2}(t)=1\middle|\,\mathcal{X}_t\right] &= 2r_{U_d} U_d^1(t)\Delta t+o(\Delta t)\\
\mathbb{P}\left[\Delta N_{U_d^2D}(t)=1\middle|\,\mathcal{X}_t\right] &= 2r_{U_d} U_d^2(t)\Delta t+o(\Delta t)
\end{aligned}
\tag{1}
$$

assuming that $\mathbb{P}[\Delta N_{XY}>1|\mathcal{X}_t]=o(\Delta t)\ \forall X,Y\in\mathcal{X}$. Note that there is no exponents in the our mathematical formulation and superscripts denote different compartments for the same stage. Branching probabilities from stage X to Y are noted $p_{Y|X}$ and rates of stay in stage X is noted r_X. The ensuing stochastic variations of the state variables are:

$$
\begin{aligned}
\Delta E(t) &= \Delta N_{SE}(t) - \Delta N_{EI^1}(t)) \\
\Delta I^1(t) &= \Delta N_{EI^1}(t) - \Delta N_{I^1I^2} \\
\Delta I^2(t) &= \Delta N_{I^1I^2} - \Delta N_{I^2I^3} \\
\Delta I^3(t) &= \Delta N_{I^2I^3} - \Delta N_{I^3I_d} - \Delta N_{I^3I_h} - \Delta N_{I^3R} \\
\Delta I_d(t) &= \Delta N_{I^3I_d} - \Delta N_{I^dR} - \Delta N_{I^dD} \\
\Delta I_h(t) &= \Delta N_{I^3I_h} - \Delta N_{I_hH_d^1} - \Delta N_{I_hH_u} - \Delta N_{I_hH_a} - \Delta N_{I_hH_b^1} \\
\Delta H_a(t) &= \Delta N_{I_hH_a} - \Delta N_{H_aR} \\
\Delta H_b^1(t) &= \Delta N_{I_hH_b^1} - \Delta N_{H_b^1H_b^2} \\
\Delta H_b^2(t) &= \Delta N_{H_b^1H_b^2} - \Delta N_{H_b^2R} \\
\Delta H_d^1(t) &= \Delta N_{I_hH_d^1} - \Delta N_{H_d^1H_d^2} \\
\Delta H_d^2(t) &= \Delta N_{H_d^1H_d^2} - \Delta N_{H_d^2D} \\
\Delta H_u(t) &= \Delta N_{I_hH_u} - \Delta N_{H_uU_d^1} - \Delta N_{H_uU_a} - \Delta N_{H_uU_b} \\
\Delta U_a(t) &= \Delta N_{H_uU_a} - \Delta N_{U_aR} \\
\Delta U_b(t) &= \Delta N_{H_uU_b} - \Delta N_{U_bR} \\
\Delta U_d^1(t) &= \Delta N_{H_uU_d^1} - \Delta N_{U_d^1U_d^2} \\
\Delta U_d^2(t) &= \Delta N_{U_d^1U_d^2} - \Delta N_{U_d^2D} \\
\Delta D(t) &= \Delta N_{I^dD} + \Delta N_{U_d^2D} + \Delta N_{H_d^2D} \\
\Delta R(t) &= \Delta N_{I^3R} + \Delta N_{I^dR} + \Delta N_{H_aR} + \Delta N_{U_aR} + \Delta N_{U_bR} \\
S(t) &= P - \sum_{X \in \mathcal{X} \setminus \{S\}} X(t),
\end{aligned}
\tag{2}
$$

where the equation for $S(t)$ enforces a constant total population.

SM Table 3: Rates of stay in each stage of the model. Some stages are composed of several compartments to accurately represent distributions shapes. For example if the rate of stay in stage U_d is r_{U_d}, then rate of stays in compartments U_d^1, U_d^2 is $2r_{U_d}$. We parameterize the model conditioning on a mean generation time of 5.2 days Ganyani et al. 2020, and an exposed and non-infectious duration of 2.9 days He et al. 2020, yielding a mean duration of 4.6 days in the infectious compartments.

Parameter	Source	Value or bound	Unit	Description
r_E	He et al. 2020	$\frac{1}{2.9}$	d^{-1}	rate of exit of the E compartment
r_I	He et al. 2020; Ganyani et al. 2020	$\frac{1}{4.6}$	d^{-1}	rate of exit of the I^1, I^2, I^3, I_d compartments
r_{I_h}	Scire et al. 2020	$\frac{1}{1.6}$	d^{-1}	rate of exit of the I_h compartment
r_{H_a}	Vaud data	$\frac{1}{3.04}$	d^{-1}	rate of exit of the H_a compartment
r_{H_b}	Vaud data	$\frac{1}{4.69}$	d^{-1}	rate of exit of the H_b^1, H_b^2 compartments
r_{H_u}	Vaud data	$\frac{1}{1.98}$	d^{-1}	rate of exit of the H_u compartment
r_{H_d}	Vaud data	$\frac{1}{3.92}$	d^{-1}	rate of exit of the H_d^1, H_d^2 compartments
r_{U_a}	Vaud data	$\frac{1}{2.94}$	d^{-1}	rate of exit of the U_a compartment
r_{U_b}	Vaud data	$\frac{1}{13.66}$	d^{-1}	rate of exit of the U_b compartment
r_{U_d}	Vaud data	$\frac{1}{3.31}$	d^{-1}	rate of exit of the U_d^1, U_d^2 compartments

SM Table 4: Branching probabilities of the model. The probability from stage A to stage B is $p_{B|A}$. There are nine different pathways from susceptible to either death or recovery. We assume that the proportion of severe infections that have sever symptoms which would require hospitalization is of 7.5%, that 50% of deaths happen outside of hospitals (data from cantons of Vaud as above and Geneva from OpenZH), that the hospitalized case fatality ratio is of 11% (data from canton of Vaud, see above), and an population-level infection fatality ratio (IFR) of 0.75 % which is in the range of published estimates Verity et al. 2020; Russell et al. 2020.

Parameter	Source	Value or bound	Description
IFR	Assumed	0.75%	Infection fatality ratio
p_s	Assumed	7.5%	Probability of severe symptoms
p_h	Deduced from Vaud data | IFR	45.4%	Probability of hospitalization
$p_{I_d\|I^3}$	Deduced from Vaud data | IFR, p_s	$p_s p_h$	
$p_{I_h\|I^3}$	Deduced from Vaud data | IFR, p_s	$p_s(1-p_h)$	
$p_{R\|I^3}$	Deduced $\|p_s$	$(1-p_s)$	
$p_{D\|I_d}$	Deduced from Vaud data | IFR, p_s	0.0916	
$p_{R\|I_d}$	Deduced from Vaud data | IFR, p_s	$1-p_{D\|I_d}$	
$p_{H_d\|I_h}$	Vaud data	$(1-0.73)\cdot(1-0.72)$	
$p_{H_u\|I_h}$	Vaud data	$(1-0.73)\cdot 0.72$	
$p_{H_a\|I_h}$	Vaud data	$0.73\cdot 0.34$	
$p_{H_b\|I_h}$	Vaud data	$0.73\cdot(1-0.34)$	
$p_{U_d\|H_u}$	Vaud data	18%	
$p_{U_a\|H_u}$	Vaud data	33%	
$p_{U_b\|H_u}$	Vaud data	34%	

3 Model Selection and Fitting/Calibration

We calibrate the model separately for each canton on the daily death and hospitalization until April 24. The calibration procedure is based on a frequentist multiple iterated filtering algorithm (MIF2 Ionides, Bretó, and King 2006). Given variations in reporting. The observation model is formulated as follows:

$$\begin{aligned} deaths(t) &\sim Poisson(\Delta D(t)) \\ \Delta hosp(t) &\sim Skellam(\Delta H(t), \Delta D_H(t) + \Delta R_H(t)) \end{aligned}$$

where, $\Delta D(t)$, $\Delta H(t)$, $\Delta D_H(t)$, $\Delta R_H(t)$ are respectively the number of new deaths, hospitalized, and deaths and discharged from hospitals at time t, ϵ is the reporting rate (between 0 and 1), k is the over-dispersion parameter of the negative binomial distribution, and $\Delta hosp(t)$ is the difference between the number of current hospitalizations at times t and $t-1$, for which we choose a Skellam distribution. The full log-likelihood of the observation model was taken as the sum of the individual log-likelihoods of the $\Delta hosp(t)$ and of the $deaths(t)$. The cases were not used as their inclusion did not refine the calibration, due to the difference in testing procedure in time.

The final parameters are shown in Table 4.

4 Assessment of Model Fit

SM Figures 5 and 6 show model fits at the national and cantonal levels respectively.

SM Table 5: Estimated values of R_0 at the beginning of the epidemic (March 01-March 10) and after the implementation of non-pharmaceutical interventions (March 29-April 5). Estimates given in terms of the median and 95% quantile range (in parenthesis).

	March 01-March 10		March 29-April 5	
Canton	median	95% QR	median	95% QR
Switzerland	3	(2.7-3.3)	0.4	(0.28-0.6)
Berne	2.2	(1.7-2.7)	0.5	(0.27-0.9)
Basel-Landschaft	3	(2.4-3.6)	0.28	(0.07-0.7)
Basel-Stadt	3.3	(2.3-4.5)	0.2	(0.04-0.7)
Fribourg	2.7	(2.2-3.3)	0.5	(0.2-0.8)
Geneva	2.6	(2.2-3.1)	0.4	(0.23-0.8)
Graubünden	1.4	(0.9-2)	0.27	(0.05-0.7)
Jura	2	(1.6-2.5)	0.5	(0.2-0.9)
Neuchatel	2	(1.7-2.4)	0.6	(0.3-1)
Ticino	2.5	(2.1-3.1)	0.5	(0.3-0.9)
Vaud	3	(2.6-3.4)	0.5	(0.29-0.8)
Valais	2.2	(1.8-2.6)	0.4	(0.15-0.7)
Zurich	2.2	(1.8-2.6)	0.5	(0.26-0.8)

SM Table 6: Estimated proportion of population infected with SARS-CoV-2 as of April 24 2020. Estimates given in terms of the median and 95% quantile range (in parenthesis).

Canton	Proportion infected [%]
Switzerland	3.0 (2.7-3.4)
Berne	1.5 (1.1-2.1)
Basel-Landschaft	3.0 (2.3-4.1)
Basel-Stadt	4.9 (3.7-6.4)
Fribourg	3.2 (2.4-4.4)
Geneva	7.8 (6.6-9.9)
Graubünden	2.0 (1.4-3.3)
Jura	2.8 (1.7-4.1)
Neuchatel	4.8 (3.6-6.4)
Ticino	14.1 (11.6-17.7)
Vaud	6.0 (5.1-7.1)
Valais	4.6 (3.6-6.5)
Zurich	1.6 (1.3-2.1)

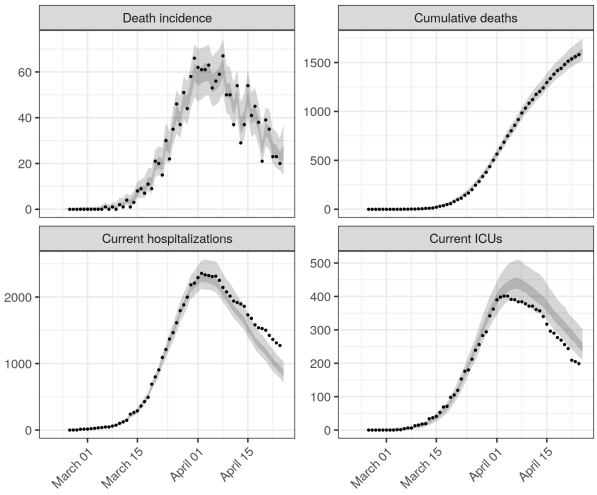

SM Figure 5: Model fit at at national level. Model results are given in terms of the 95% (light gray) and 50% quantile ranges of the smoothing distribution of R_0 at the maximum likelihood estimates of inferred parameters. Data (points) from Probst 2020

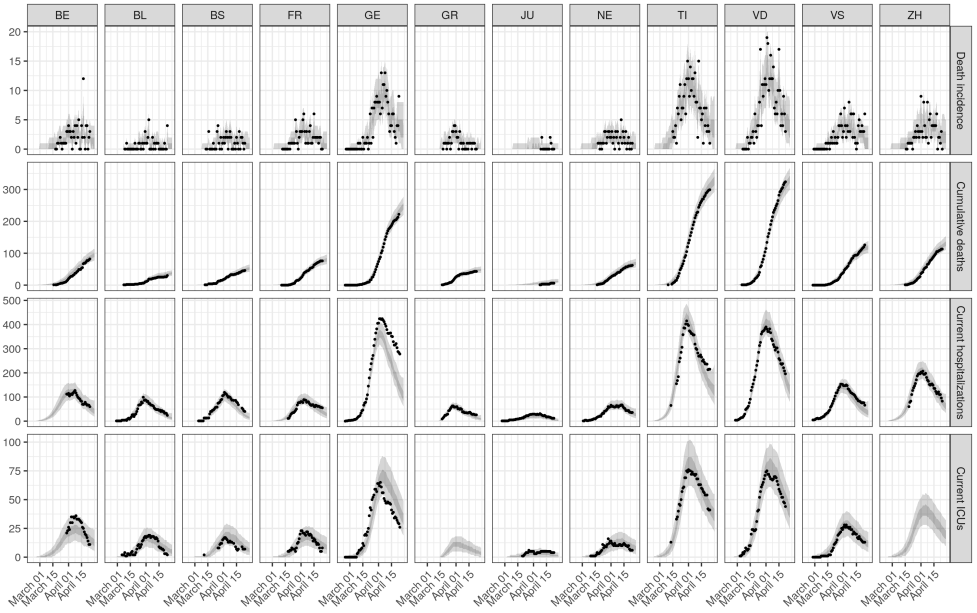

SM Figure 6: Cantonal level fits. Legend as in SM Figure 5. Data (points) from openZH 2020.

5 Mobility analysis

SM Figure 7 explores the cross-cantonal correlation between reduction in R_0 and mobility changes.

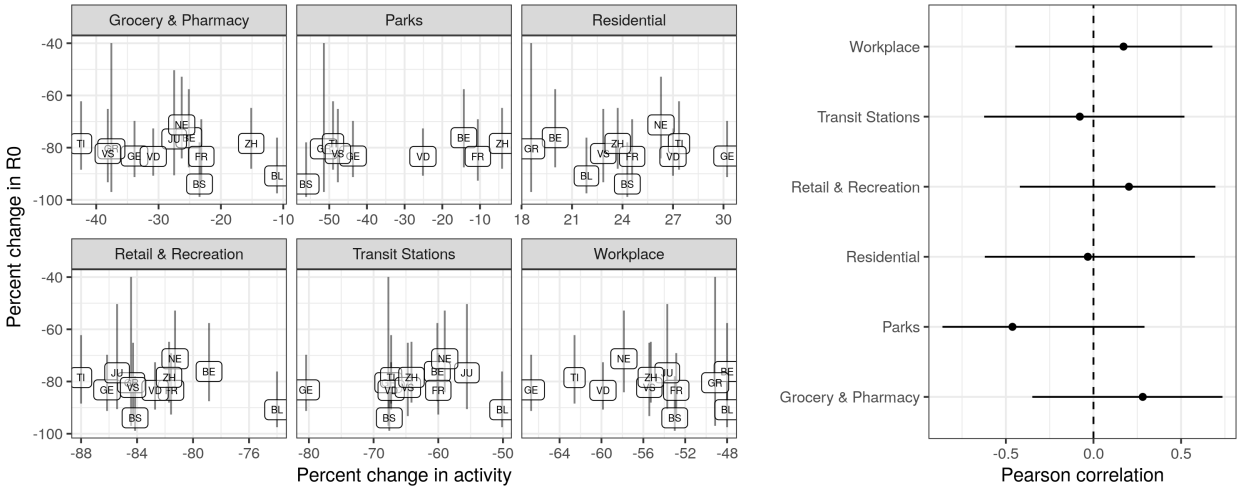

SM Figure 7: Cross-cantonal association between reductions in R_0 and activity-related mobility. Left: Scatter plots of maximal reduction in activity against maximal estimated reduction in R_0, vertical error bars indicate the 95% quantile range of R_0. Right: correlation coefficients per activity.

6 Changepoint analysis

We used Bayesian changepoint models to infer dates of changes in R0 reduction using the *mcp* package in R Lindeløv 2020. We test both models with one, two and three segments between two intercepts to cover possible changes in the speed of decrease of R0 between assuming stable baseline and final post-NPI states as observed in exploratory analysis. We used Bayesian leave-one-out cross-validation to select the number of changepoints Vehtari, Gelman, and Gabry 2017.

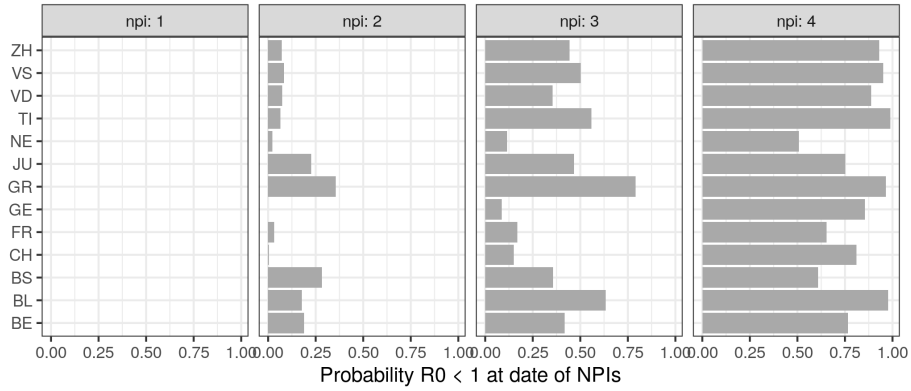

SM Figure 8: Cantonal-level probability that R_0 was below one at dates of NPIs. National scale probability denoted by 'CH'. NPI numbers correspond to 1) Ban of events of more than 1000 people on February 28, 2) School closure on March 13, 3) Closure of all non-essential commercial activities on March 16, 4) Ban of gatherings of more than 5 people and recommended home isolation on March 20.

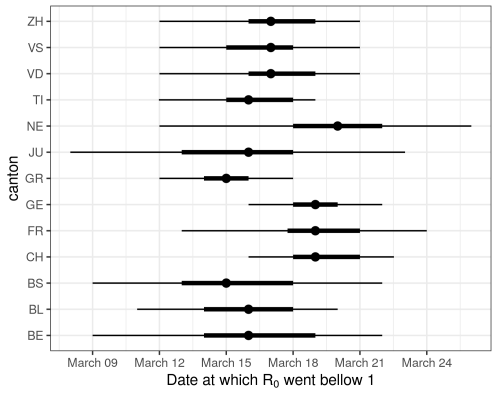

SM Figure 9: Date at which R_0 fell below 1. Estimates are shown in terms of the median (point), IQR (thick error bars) and 95% quantile range (error bars). National crossing date denoted by 'CH'.

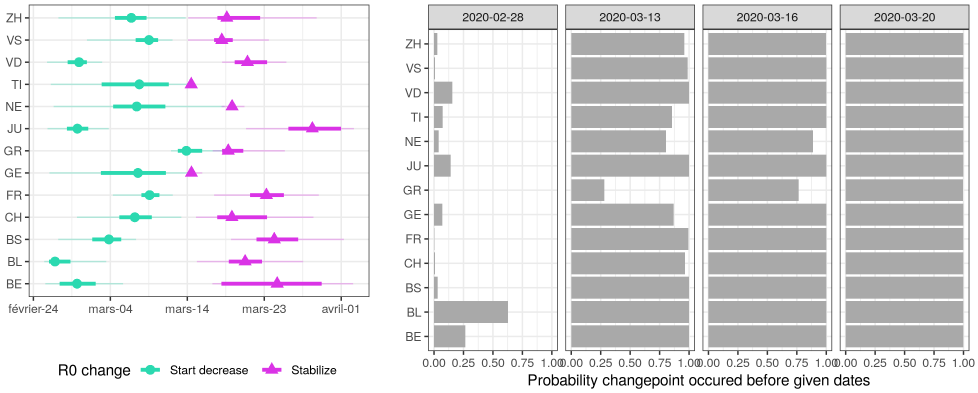

SM Figure 10: Changepoints of R_0 and dates of NPIs. Left: Dates of initiation and stabilization of reduction in R_0 based on changepoint models with single slope in terms of the median (points), IQRs (thick error bars) and 95% quantile ranges (error bars). Right: Posterior probabilities that R_0 started decreasing before the date of implementation of NPIs as described in Figure 1 of the main text. National-level estimates are denoted by 'CH'.

SM Table 7: Model comparison results of changepoint models applied to estimated R_0 time series. We considered models with two plateaus connected by either one (model1), two (model2) or three (model3) distinct slopes. Model comparison was performed by Bayesian leave-one-out cross-validation Vehtari, Gelman, and Gabry 2017. Difference in estimated log pointwise predictive density (elpd) between two models are considered significant if their absolute value is larger than 5 times their standard error (SE). The best fitting model is ordered first for each canton. National scale models denoted by 'CH'.

Canton	Model	elpd difference	SE	significant
BE	model3	0.0000000	0.0000000	
BE	model2	-0.6675670	1.2140749	FALSE
BE	model1	-94.8766837	12.1712432	TRUE
BL	model3	0.0000000	0.0000000	
BL	model2	-0.2864307	0.4527180	FALSE
BL	model1	-8.9822685	2.1418540	FALSE
BS	model3	0.0000000	0.0000000	
BS	model2	-2.5160741	0.8680027	FALSE
BS	model1	-205.6078012	22.6092620	TRUE
CH	model3	0.0000000	0.0000000	
CH	model2	-63.7843668	12.0206299	TRUE
CH	model1	-63.8752597	16.2223803	FALSE
FR	model3	0.0000000	0.0000000	
FR	model2	-4.7053226	2.1881538	FALSE
FR	model1	-12.1537456	6.1634667	FALSE
GE	model3	0.0000000	0.0000000	
GE	model2	-9.1269377	5.4125328	FALSE
GE	model1	-21.9255808	9.0988603	FALSE
GR	model3	0.0000000	0.0000000	
GR	model2	-5.3913506	4.6699981	FALSE
GR	model1	-73.8487168	13.1231392	TRUE
JU	model2	0.0000000	0.0000000	
JU	model3	-47.0447743	7.2033450	TRUE
JU	model1	-53.7500523	9.3085257	TRUE
NE	model3	0.0000000	0.0000000	
NE	model2	-8.2987815	4.4514442	FALSE
NE	model1	-19.3360196	6.5748078	FALSE
TI	model3	0.0000000	0.0000000	
TI	model2	-48.6373831	8.7871880	TRUE
TI	model1	-65.4690638	14.8095040	FALSE
VD	model3	0.0000000	0.0000000	
VD	model1	-40.4790495	16.2094131	FALSE
VD	model2	-60.3699654	6.6993957	TRUE
VS	model3	0.0000000	0.0000000	
VS	model2	-13.8340777	3.8148460	FALSE
VS	model1	-22.0766069	5.1957260	FALSE
ZH	model2	0.0000000	0.0000000	
ZH	model3	-23.2795225	5.4139018	FALSE
ZH	model1	-31.6578508	5.8042425	TRUE

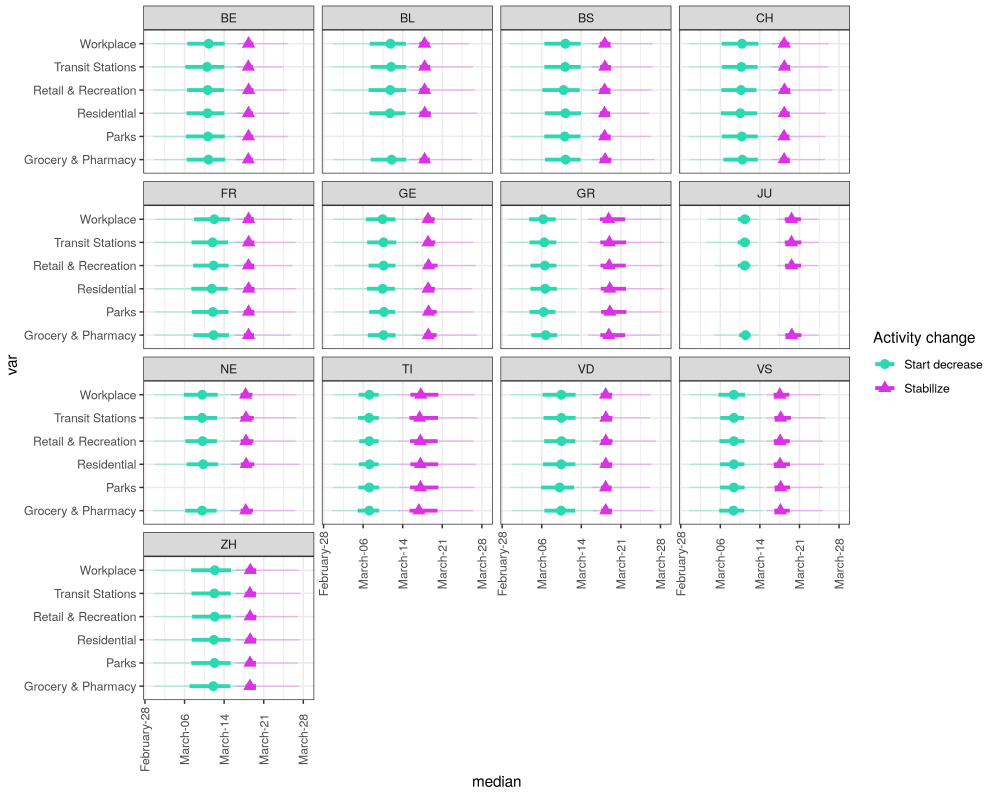

SM Figure 11: Changpoints in activity-related mobility. Dates of initiation and stabilization of reduction in each type of mobility based on changepoint models with single slope in terms of the median (points), IQRs (thick error bars) and 95% quantile ranges (error bars). National-level estimates are in panel 'CH'.

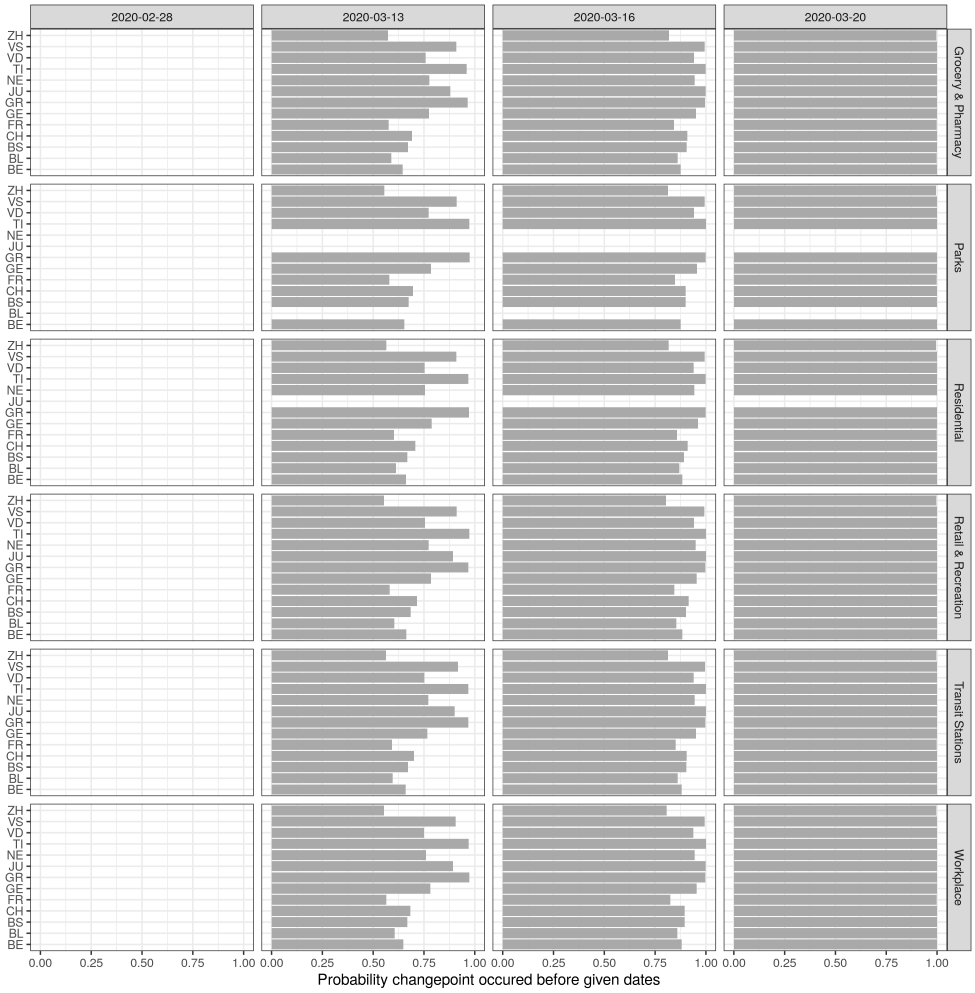

SM Figure 12: Posterior probabilities that activity-related mobility started decreasing before the date of implementation of NPIs as described in Figure 1 of the main text. National-level estimates are denoted by 'CH'.

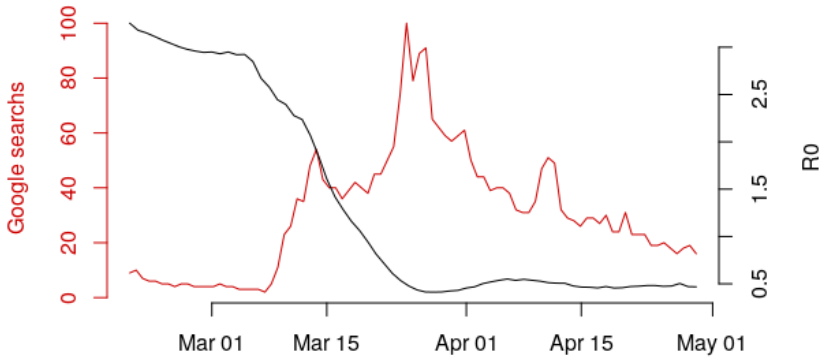

SM Figure 13: Google trends for COVID-19 and changes in R_0 in Switzerland. Trends corresponds to the keyword "coronavirus" (red line), time evolution of R_0 from the main text.

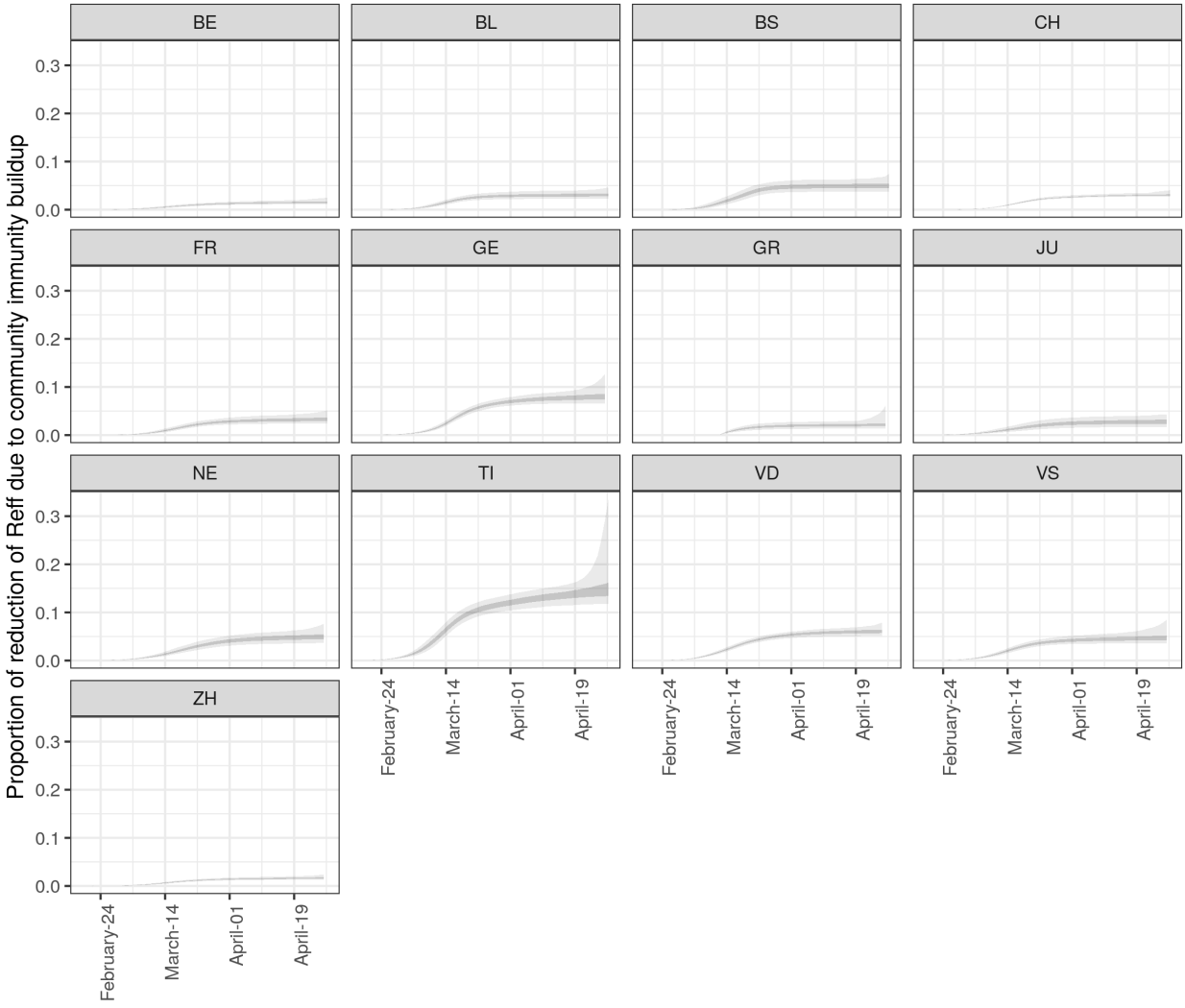

SM Figure 14: Proportion the reduction in the effective reproduction number R_{eff} linked to depletion of susceptibles due to buildup of community immunity.

References

Bretó, Carles et al. (Mar. 2009). "Time series analysis via mechanistic models". In: *The Annals of Applied Statistics* 3.1, pp. 319–348. ISSN: 1932-6157, 1941-7330. DOI: 10.1214/08-AOAS201. URL: https://projecteuclid.org/euclid.aoas/1239888373 (visited on 06/27/2019).

Carpenter, Bob et al. (Jan. 11, 2017). "Stan: A Probabilistic Programming Language". In: *Journal of Statistical Software* 76.1. Number: 1, pp. 1–32. ISSN: 1548-7660. DOI: 10.18637/jss.v076.i01. URL: https://www.jstatsoft.org/index.php/jss/article/view/v076i01 (visited on 05/02/2020).

Ganyani, Tapiwa et al. (Mar. 8, 2020). "Estimating the generation interval for COVID-19 based on symptom onset data". In: *medRxiv*. Publisher: Cold Spring Harbor Laboratory Press, p. 2020.03.05.20031815. ISSN: 10.1101/2020.03.05.20031815. DOI: 10.1101/2020.03.05.20031815. URL: https://www.medrxiv.org/content/10.1101/2020.03.05.20031815v1 (visited on 04/25/2020).

He, Xi et al. (Apr. 15, 2020). "Temporal dynamics in viral shedding and transmissibility of COVID-19". In: *Nature Medicine*. Publisher: Nature Publishing Group, pp. 1–4. ISSN: 1546-170X. DOI: 10.1038/s41591-020-0869-5. URL: https://www.nature.com/articles/s41591-020-0869-5 (visited on 04/25/2020).

Ionides, Edward L., C. Bretó, and Aaron. A. King (Dec. 5, 2006). "Inference for nonlinear dynamical systems". In: *Proceedings of the National Academy of Sciences* 103.49, pp. 18438–18443. ISSN: 0027-8424, 1091-6490. DOI: 10.1073/pnas.0603181103. URL: https://www.pnas.org/content/103/49/18438 (visited on 05/06/2019).

King, Aaron A. et al. (Aug. 2008). "Inapparent infections and cholera dynamics". In: *Nature* 454.7206, p. 877. ISSN: 1476-4687. DOI: 10.1038/nature07084. URL: https://www.nature.com/articles/nature07084 (visited on 12/21/2017).

Lindeløv, Jonas Kristoffer (Jan. 5, 2020). *mcp: An R Package for Regression With Multiple Change Points*. preprint. Open Science Framework. DOI: 10.31219/osf.io/fzqxv. URL: https://osf.io/fzqxv (visited on 04/29/2020).

Nishiura, Hiroshi et al. (Aug. 31, 2009). "Early Epidemiological Assessment of the Virulence of Emerging Infectious Diseases: A Case Study of an Influenza Pandemic". In: *PLOS ONE* 4.8. Publisher: Public Library of Science, e6852. ISSN: 1932-6203. DOI: 10.1371/journal.pone.0006852. URL: https://journals.plos.org/plosone/article?id=10.1371/journal.pone.0006852 (visited on 05/01/2020).

openZH (Apr. 25, 2020). *openZH/covid_19*. original-date: 2020-03-09T10:07:28Z. URL: https://github.com/openZH/covid_19 (visited on 04/25/2020).

Probst, Daniel (May 2, 2020). *daenuprobst/covid19-cases-switzerland*. original-date: 2020-03-12T12:09:53Z. URL: https://github.com/daenuprobst/covid19-cases-switzerland (visited on 05/02/2020).

Russell, Timothy W. et al. (Mar. 26, 2020). "Estimating the infection and case fatality ratio for coronavirus disease (COVID-19) using age-adjusted data from the outbreak on the Diamond Princess cruise ship, February 2020". In: *Eurosurveillance* 25.12. Publisher: European Centre for Disease Prevention and Control, p. 2000256. ISSN: 1560-7917. DOI: 10.2807/1560-7917.ES.2020.25.12.2000256. URL: https://www.eurosurveillance.org/content/10.2807/1560-7917.ES.2020.25.12.2000256 (visited on 05/02/2020).

Scire, Jérémie et al. (2020). "Monitoring COVID-19 spread in Switzerland". Library Catalog: bsse.ethz.ch. URL: https://bsse.ethz.ch/cevo/research/sars-cov-2/real-time-monitoring-in-switzerland.html (visited on 04/26/2020).

Vehtari, Aki, Andrew Gelman, and Jonah Gabry (Sept. 1, 2017). "Practical Bayesian model evaluation using leave-one-out cross-validation and WAIC". In: *Statistics and Computing* 27.5. Company: Springer Distributor: Springer Institution: Springer Label: Springer Number: 5 Publisher: Springer US, pp. 1413–1432. ISSN: 1573-1375. DOI: 10.1007/s11222-016-9696-4. URL: https://link.springer.com/article/10.1007/s11222-016-9696-4 (visited on 05/01/2020).

Verity, Robert et al. (Mar. 30, 2020). "Estimates of the severity of coronavirus disease 2019: a model-based analysis". In: *The Lancet Infectious Diseases*. ISSN: 1473-3099. DOI: 10.1016/S1473-3099(20)30243-7. URL: http://www.sciencedirect.com/science/article/pii/S1473309920302437 (visited on 05/02/2020).